

Dielectric properties of copper phthalocyanine nanocomposites incorporated with graphene oxide

Zicheng Wang¹ · Renbo Wei¹ · Xiaobo Liu¹

Received: 12 December 2016 / Accepted: 18 January 2017 / Published online: 8 February 2017
© Springer Science+Business Media New York 2017

Abstract Graphene/phthalocyanine derivatives were successfully prepared by self-assembling of phthalocyanine on graphene sheets under solvothermal condition. The results of Ultraviolet Visible (UV–Vis), X-ray photoelectron spectroscopy, scanning electron microscope and electrical measure suggested that the competition between metal–ligand coordination and π – π interaction between graphene and phthalocyanine endowed composites with conspicuous evolutions in self-assembly behavior, morphology and dielectric properties. Importantly, the effective restoration of π -electron within the graphene played a dominant role in enhancing the dielectric properties of the system while the formation of metal–ligand coordination bond between graphene oxide and copper phthalocyanine hindered the improvement of dielectric properties.

1 Introduction

As a class of porphyrin derivative, copper phthalocyanine (CuPc) has been successfully fabricated into special architectures (microsphere, nanofiber, nanowire and nanothorn) through the intimate packing of the aromatic heterocycles [1–4] and has received increasing attention due to its potential applications [5–8]. However, the relatively low intrinsic dielectric constant (~ 4) of CuPc limits its further application in capacitors. Up to now, many studies have been attempted to improve this property [9–11]. Recently, graphene and/or graphene oxide (GO) have been employed to enhance the dielectric properties of CuPc due to the remarkable electrical properties of graphene [12, 13]. However, with a deeper investigation in this system, we found that beside the π – π interaction between CuPc and GO, the oxygen-functional groups of GO, especially the carboxyl and epoxy species, tend to act as a ligand that coordinated with the central metal ions on CuPc [14, 15].

In this paper, in order to investigate the effect of competition between metal–ligand coordination and π – π interaction on the self-assembly behavior, morphology and dielectric properties of GO/CuPc nanocomposites, GO/CuPc, RGO (reduced graphene oxide)/CuPc and GO/H₂Pc (metal-free phthalocyanine) were fabricated and treated under solvothermal condition. For GO/CuPc, both of the metal–ligand coordination and π – π interaction existed. For comparison, the metal–ligand coordination was weakened as the removing of epoxy groups while the π – π interaction was strengthened as the restoration of the π -electron system of RGO in RGO/CuPc. GO/H₂Pc was only controlled by π – π interaction as the absence of Cu in H₂Pc. The self-assembly behaviors, morphology and dielectric properties of the nanocomposites will be studied in detail.

Zicheng Wang and Renbo Wei have contributed equally to this work.

Electronic supplementary material The online version of this article (doi:10.1007/s10854-017-6433-5) contains supplementary material, which is available to authorized users.

✉ Renbo Wei
weirb10@uestc.edu.cn

✉ Xiaobo Liu
liuxb@uestc.edu.cn

¹ Research Branch of Advanced Functional Materials, Institute of Microelectronic & Solid State Electronic, High-Temperature Resistant Polymers and Composites Key Laboratory of Sichuan Province, University of Electronic Science & Technology of China, Chengdu 610054, People's Republic of China

2 Experimental

2.1 Materials

Graphite powder (325 mesh, Qingdao Jin Ri Lai Graphite Co. Ltd., Qingdao, China). 4, 4'-bis (3, 4-dicyanophenoxy) biphenyl (BPH) was synthesized in our laboratory. 4, 4'-Diaminediphenyl sulfone (DDS, as curing agent) was purchased from Sichuan Dongcai chemicals. Cuprous chloride (CuCl), *N,N*-Dimethylformamide (DMF), *N*-methyl-2-pyrrolidone (NMP) and *N,N*-dimethylacetamide (DMAc) were supplied by Tianjin BODI chemicals, Tianjin, China. All the materials were used without any further purification.

2.2 Preparation of copper phthalocyanine (U-CuPc)

1.31 g (3 mmol) BPH and 0.10 g (1 mmol) CuCl were dissolved in 40 mL of DMAc and then the mixture was stirred at 160 °C for 4 h, and then the solution was cooled to room temperature. The crude product was collected by filtration, washed with water, and dried in vacuum. After refluxing in methanol twice, the product was filtrated and washed using cold methanol for three times. The blue powdery product was dried in vacuum. The preparation process of CuPc was illustrated in Figure S1. ¹H NMR (300 MHz, DMSO-*d*₆) (Figure S2), δ (ppm): 8.15–8.00 (m), 7.86–7.61 (m), 7.44–7.32 (m), 7.31–7.13 (m). FTIR (KBr, cm⁻¹ Figure S3): 3432, 2231, 1730, 1605, 1489, 1289, 1090. UV–Vis (NMP, nm Figure S4): $\lambda_{\max 1}$ = 679, $\lambda_{\max 2}$ = 613. Content of phthalocyanine ring in CuPc was calculated as 10.7% (Figure S4). TGA: 415 °C (5% weight loss) (Figure S5); GPC: M_n = 2317, M_w/M_n = 1.41.

2.3 Preparation of metal-free phthalocyanine (U-H₂Pc)

First, Bph monomer (5 g) was dissolved in 5 mL of NMP and then, DDS (0.1 g, 2 wt%) was added slowly with being stirred vigorously at 200 °C for 2 h, giving a dark green solution. The crude product was collected by filtration, washed with hot water, and dried in vacuum. After refluxing in methanol twice, the product was filtrated and washed using cold methanol for three times. The blue powdery product was dried in vacuum. The preparation process of H₂Pc was illustrated in Figure S6. ¹H NMR (300 MHz, DMSO-*d*₆ Figure S7), δ (ppm): 8.12–8.08 (m), 7.85–7.76 (m), 7.45–7.40 (m), 7.28–7.25 (m). FTIR (KBr, cm⁻¹ Figure S8): 3440, 2230, 1740, 1590, 1490, 1250, 1090, 1010, 949, 835, 716. UV–Vis (NMP, nm Figure S9): $\lambda_{\max 1}$ = 671, $\lambda_{\max 2}$ = 702. TGA (Figure S10): 421 °C (5% weight loss). GPC: M_n = 2023, M_w/M_n = 1.51.

2.4 Preparation of graphene oxide (GO)

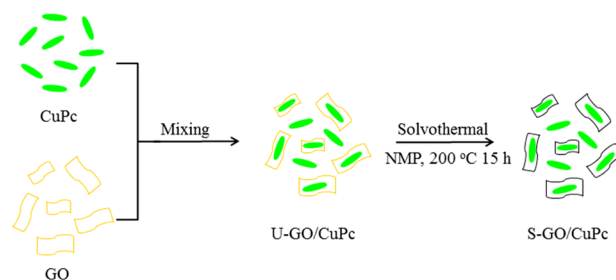
GO was prepared from graphite powder through an improved Hummer's method as reported [16].

2.5 Preparation of graphene oxide/copper phthalocyanine (GO/CuPc) nanocomposites

An aqueous graphene oxide suspension was generated by sonication (1 h) of 40 mg GO (40 mL NMP) in a three-necked round bottom flask reactor. After addition of 760 mg CuPc (40 mL NMP) with vigorous mechanical stirring for 24 h, the back-green suspensions of GO/CuPc was obtained, resulting a concentration of 0.5 mg/mL GO and 9.5 mg/mL CuPc. A part of the suspensions was filtered over a 0.2 μ m PTFE microporous membrane, and dried at 80 °C in vacuum. The obtained powders of GO/CuPc nanocomposites were marked as **U-GO/CuPc** as depicted in Scheme 1. Meanwhile, the other part of the suspensions was sealed in a Teflon lined stainless-steel autoclave. The autoclave was maintained at 200 °C for 15 h with dispersions up to 80% of the total volume, and cooled to room temperature naturally. The crude products were collected by filtration, washed with water, and dried at 80 °C in vacuum. After heating treatment, the obtained samples were labeled as **S-GO/CuPc**. In addition, for exploring reduction mechanism of GO under solvothermal condition, 0.5 mg/mL GO suspensions without CuPc in NMP was also sealed in Teflon lined stainless-steel autoclave and treated with the same process. The final products were named as **RGO-S**.

2.6 Preparation of reduced graphene oxide/copper phthalocyanine (RGO/CuPc) nanocomposites

The RGO/CuPc nanocomposites with 5 wt% GO were prepared as follow: GO (40 mg) was loaded in a 250 mL round bottom flask and the 128 mL solvent mixture



Scheme 1 Illustration of the procedure to prepare the GO/CuPc nanocomposites

of H₂O and DMF (volume ratio DMF: H₂O=9:1) was then added with vigorous mechanical stirring and sonication for 2 h, yielding a homogeneous suspensions of the graphene oxide sheets [17]. Hydrazine monohydrate (13 μ L) was subsequently added to the suspensions with additional stirring at 80 °C for 12 h, yielding black suspensions. The corresponding products were denoted as **RGO-H** or **RGO** (as a default). After cooling to room temperature, the solution of 760 mg CuPc (20 mL DMF) was dropped into the RGO suspensions with vigorous mechanical stirring for 24 h. The suspensions was filtered over a 0.2 μ m PTFE microporous membrane, and dried at 80 °C in vacuum. The obtained powders of RGO/CuPc nanocomposites were marked as **U-RGO/CuPc**. Meanwhile, the RGO/CuPc nanocomposites were dispersed in NMP, yielding a concentration of 9.5 mg/mL CuPc, and then sealed in a Teflon lined stainless-steel autoclave. The autoclave was maintained at 200 °C for 15 h with dispersions up to 80% of the total volume, and cooled to room temperature naturally. The crude products were collected by filtration, washed with water, and dried at 80 °C in vacuum. The powders of RGO/CuPc nanocomposites were labeled as **S-RGO/CuPc**. The procedure to prepare the S-RGO/CuPc was similar to that of S-GO/CuPc as displayed in Scheme 1.

2.7 Preparation of graphene oxide/metal-free phthalocyanine (GO/H₂Pc) nanocomposites

The procedure to prepare the S-GO/H₂Pc was similar to that of S-GO/CuPc as depicted in Scheme 1. The obtained nanocomposites of GO and H₂Pc were marked as **U-GO/H₂Pc**. After the solvothermal treatment, the obtained samples were labeled as **S-GO/H₂Pc**. For comparing with the nanocomposites, the pure CuPc (9.5 mg/mL, NMP) and H₂Pc (9.5 mg/mL, NMP) were also treated by using the similar procedure and conditions (200 °C for 15 h), and the final products were denoted as **S-CuPc** and **S-H₂Pc**, respectively.

2.8 Characterization

Nuclear Magnetic Resonance (¹H NMR) spectrum was recorded on a JEOL JNM-AL spectrometer (300 MHz). Fourier transform infrared (FTIR) measurement was carried out on a Shimadzu 8400S FTIR spectrophotometer by incorporating the samples in the KBr pellets. Ultraviolet–visible spectroscopy absorption spectra were obtained on a UV2501-PC spectrophotometer. The molecular weights and molecular weight distributions were measured using a gel permeation chromatographic (GPC) instrument equipped with a styragel @ HR column and a refractive index (RI) detector (Waters 2414). Thermal Gravimetric

Analyzer (TGA) analysis was carried out using TA Q50 system under nitrogen atmosphere at a heating rate of 20 °C/min. X-ray photoelectron spectroscopic (XPS) measurements were carried out on ESCA 2000 (VG Microtech, UK) using a monochromic Al K α ($h\nu = 1486.6$ eV) X-ray source. X-ray diffraction (XRD) patterns were recorded on a Rigaku RINT 2400 with Cu K α . Dielectric measurements were carried out by an Agilent 4284A dielectric analyser. Scanning electron microscopic (SEM) images were taken on a JSM 6490LV (JEOL, Japan) field emission microscope. Dielectric and alternating current (AC) conductivity measurements were carried out by an Agilent 4284A dielectric analyser.

3 Results and discussion

In this study, the graphene/phthalocyanine nanocomposites were fabricated, as illustrated in Scheme 1. Firstly, the nanocomposites were fabricated by self-assembling of phthalocyanine molecule on graphene sheets through π – π interaction and metal–ligand coordination between graphene and phthalocyanine. Secondly, the obtained composites were further treated during the solvothermal reduction process for investigating the effect of the formation of metal–ligand coordination and restoration of π -electron within the graphene on the self-assembly behaviors, morphology and dielectric properties of phthalocyanine.

3.1 Reduction of graphene oxide

In this paper, two methods were utilized to reduce GO, involving hydrazine monohydrate and solvothermal reduction. Before incorporated into CuPc matrix, GO sheets were reduced by using hydrazine monohydrate for removing epoxy groups in the surface of graphene oxide sheets, which tend to act as a ligand that coordinated with the central copper ions on CuPc. For comparing with GO/CuPc and GO/H₂Pc, the decrease of epoxy groups in RGO will weaken the metal–ligand coordination and strengthen the π – π interaction between RGO and CuPc as the restoration of the π -electron system, which will significantly influence the self-assembly behaviors, morphology and dielectric properties of the graphene/phthalocyanine nanocomposites. After fabrication of nanocomposites, solvothermal reduction process was employed to explore the effect of the formation of metal–ligand coordination bond on the reduction of oxygen-functional groups in GO sheets, thereby corresponding to the changes in the self-assembly behaviors, morphology and dielectric properties of those composites. Therefore, in order to further understand the reduction mechanism of GO without the disturbance of phthalocyanine molecules, the pure GO sheets were treated

by using hydrazine monohydrate as reductant and under solvothermal conditions, respectively.

XRD measurements were performed to study the changes in structure of GO. As recorded in Fig. 1, the initial GO powder shows a sharp diffraction peak (001) centered at $2\theta=10.46^\circ$, corresponding to an interlayer spacing of 8.45 Å [16]. In comparison to the natural graphite (d -spacing 3.37 Å at $2\theta=26.45^\circ$), this 5.08 Å expansion of d -spacing can be attributed to the effective intercalation of oxygen-functional groups into graphite interlayers, thereby achieving the complete exfoliation of graphene sheets. After the reduction, the characteristic diffraction peak (001) of RGO-H and RGO-S disappears completely while a new broad diffraction peak about 23.52° (d -spacing 3.78 Å) and 25.18° (d -spacing 3.54 Å) appears, respectively, which is closer to the typical (002) diffraction peak of graphite. The drastic evolution in XRD patterns demonstrates that solvothermal reduction as well as hydrazine monohydrate is an efficient approach in removal of oxygen-functional groups from GO sheets and restoration of the graphite structure [18].

To gain more details about the surface chemical changing of GO during the reduction process, the samples were also characterized by XPS, as shown in Fig. 2. Two obvious peaks can be observed at 287 and 534.5 eV in the XPS spectrum of GO, RGO-H, and RGO-S, corresponding to C1s and O1s, respectively (Fig. 2a). As calculated, the area ratio of C1s peak and O1s peak (C/O ratio) of GO (2.04), RGO-H (3.33), and RGO-S (4.18) displays a tendency to gradually increase, revealing the efficiency in reduction of GO by using hydrazine monohydrate and/or under

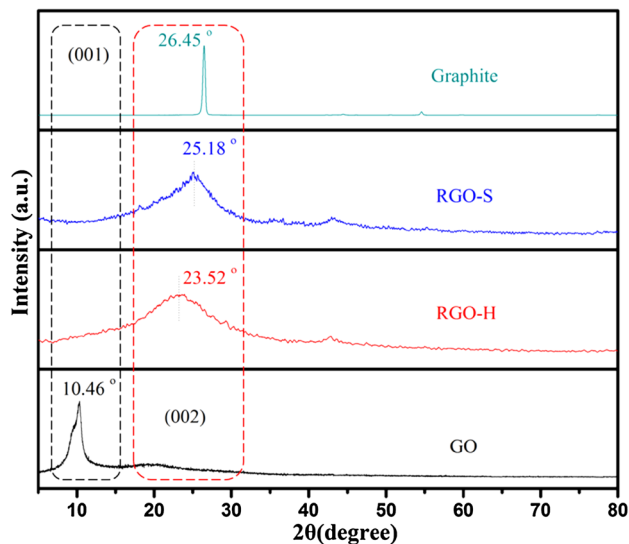


Fig. 1 XRD patterns of GO, RGO-H (reduced by hydrazine monohydrate for 12 h), RGO-S (reduced under solvothermal conditions at 200 °C for 15 h) and Graphite

solvothermal treatment. Moreover, the C1s spectrum of GO could be quantitatively differentiated into four different carbon species (O=C–O, C=O, C–O–C (epoxy/ether), C–OH and C=C), as shown in Fig. 2b [19]. After the reaction with hydrazine monohydrate at 80 °C for 12 h, a distinct decrease on the atomic percentage of C–O–C peak at 286.79 eV can be observed (Fig. 2c; Table 1), indicating that epoxy groups on the surface of GO have been effectively consumed by the reductant, leading to the obvious increase in C/O ratio as shown in Fig. 2a. As a result, it will further change the interaction between graphene sheets and phthalocyanine molecules. Importantly, after the solvothermal treatment, hydroxyl groups (C–OH) also exhibit dramatically decrease besides epoxy groups, leading to the further increase of C/O ratio. Thus, it can be concluded that the solvothermal process is more effectively and powerfully method for reducing GO than that by using hydrazine monohydrate as reductant, which will play a dominant role in removing of the hydroxyl and epoxy groups on GO sheets without any disturbances.

3.2 XPS spectra of the graphene/phthalocyanine nanocomposites

In order to investigate the effect of solvothermal conditions on the metal–ligand coordination bond between GO and CuPc, the Cu 2p spectrum has been further analyzed as shown in Fig. 3. It can be obviously observed that the Cu 2p spectra has two strong peaks, one located at ~ 952.8 eV and another located at ~ 932.8 eV, corresponding to the electron states of Cu $2p_{1/2}$ and Cu $2p_{3/2}$, respectively. The binding energy (932.8 eV) of copper atoms in Cu $2p_{3/2}$ electron state corresponds to the oxidation state of Cu element in CuPc system [20, 21]. In the CuPc molecule, the Cu species with multiplet splitting satellite bonded with nitrogen atoms through coordinate bonds. For U-GO/CuPc, a 0.12 eV shifts on Cu $2p_{3/2}$ signal after incorporation of 5 wt% GO into CuPc (from 932.91 to 932.79 eV). The down-shift in binding energy indicates the charge transfers from GO to CuPc in the composite because the binding energy is related to the electron density around the Cu nucleus. The lower the binding energy is, the higher the electronic density. It can be ascribed to the formation of metal–ligand coordination bond between the oxygen-functional groups of GO, especially the carboxyl and epoxy groups, and the central metal ions of CuPc, leading to the increase of electron density around the Cu nucleus. The changes directly confirms the existence of metal–ligand coordination bond between GO and CuPc. After treated under solvothermal conditions, normally, the decomposition of labile oxygen functional groups results in the restoration of the π -conjugated network within the graphene, effectively enhancing π – π interaction with CuPc. For the

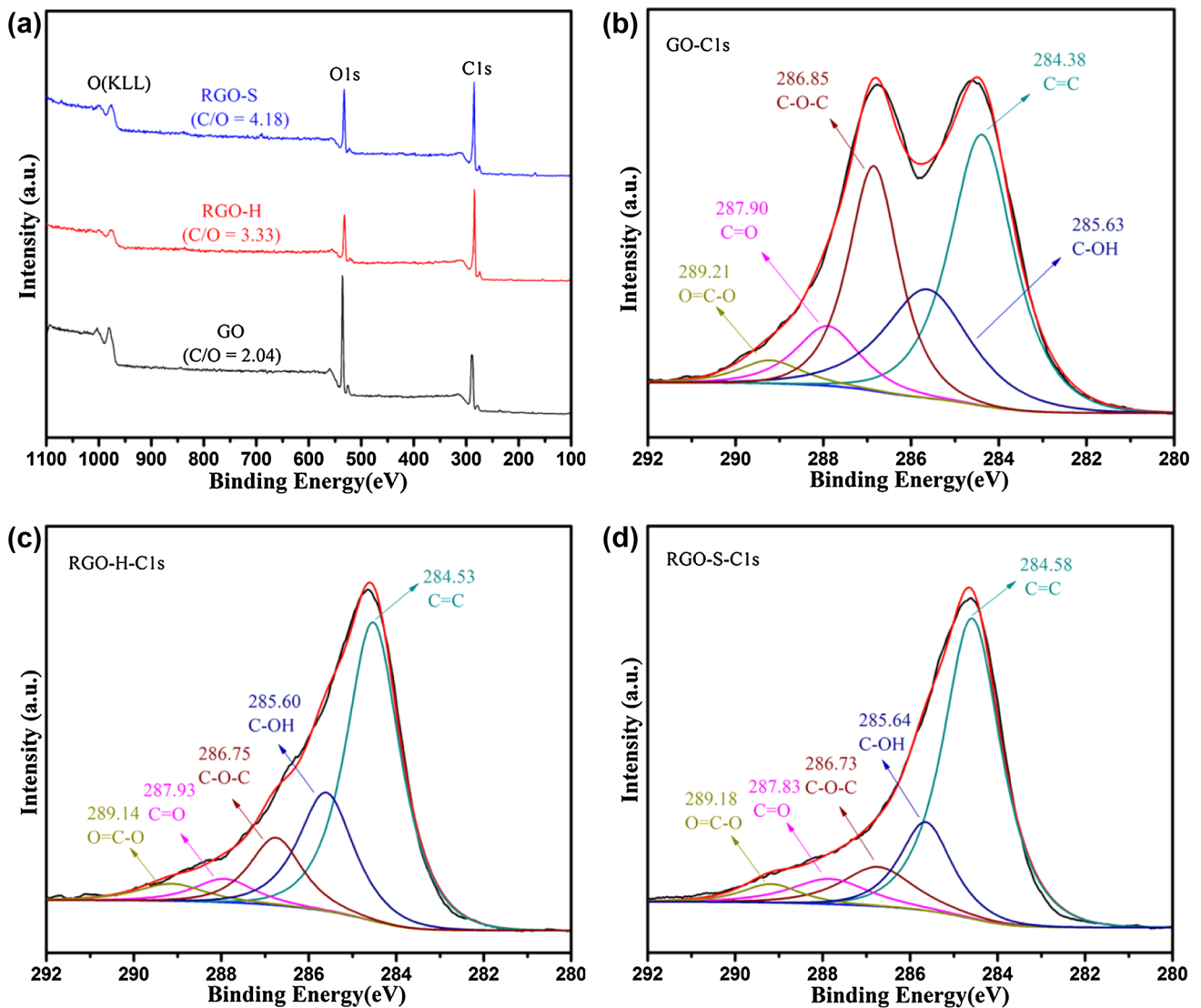


Fig. 2 XPS survey spectra of GO, RGO-H, and RGO-S (a); high-resolution C1s XPS spectra of GO, RGO-H, and RGO-S, respectively

Table 1 Carbon atomic percentage (at%) of various chemical states in GO, RGO-H and RGO-S

	O=C-O	C=O	C-O-C	C-OH	C=C
GO	3.37	8.72	26.32	21.48	40.11
RGO-H	4.03	4.91	12.27	22.76	56.03
RGO-S	4.98	5.00	11.18	15.81	63.01

central Cu ions of CuPc, the electron density around the Cu nucleus subsequently decreases due to the delocalization effect of π -electron within phthalocyanine ring, leading to the increase in binding energy, as reported by Chunder [22]. However, on the contrary, the binding energy continuously decreases to 932.55 eV for S-GO/CuPc. For the system, the abnormality in binding energy exactly verifies the

existence of metal–ligand coordination bond between GO and CuPc. As a kind of special covalent bond, the formation of metal–ligand coordination bond will strengthen the oxygen-functional groups, which hinders the breakaway of them during the process of heating treatment. But the other uncoordinated oxygen-functional groups, hydroxyl groups, can successfully break away under solvothermal conditions (200 °C 15 h), resulting in the restoration of local delocalized π -electron system of GO. For S-GO/CuPc, the decrease in binding energy, namely the increase of the electron density around the Cu nucleus, which may be attributed to that the part restoration of local delocalized π -electron system of GO sheets effectively enhances the electron density within GO sheets, leading to increment of electron density of coordinated electrophilic oxygen-functional groups. As a result, the restriction of shared electrons

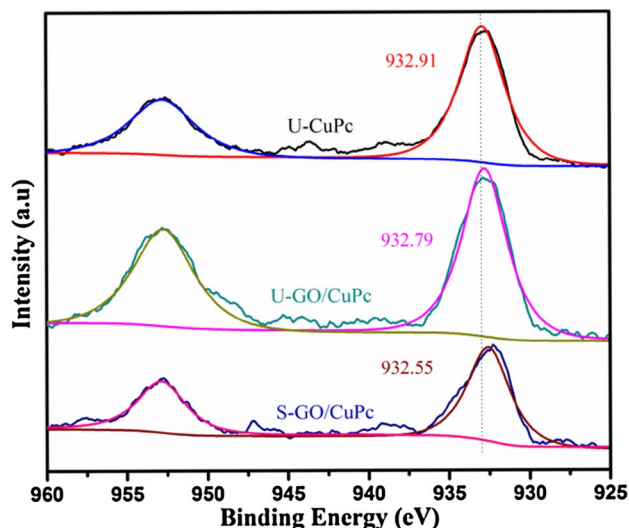


Fig. 3 High resolution Cu 2p XPS spectra of U-CuPc, U-GO/CuPc and S-GO/CuPc

pairs in metal–ligand coordination bond derived from oxygen-functional groups weakens, which shifts to Cu nucleus with unoccupied orbital, leading to increment of electron density around the Cu nucleus.

3.3 UV–Vis spectra of the graphene/phthalocyanine nanocomposites

UV–Vis spectrophotometer was employed to trace the changing interaction in the composites. A distinct absorption band arises at ~680 nm as shown in Fig. 4a, which can be assigned to the characteristic Q-band absorption of CuPc [23]. The Q-band of U-GO/CuPc is almost the same as that of CuPc while the Q-band absorption peak of U-RGO/CuPc shows an obvious red-shift compared with that of CuPc, which can be ascribed to the enhanced π – π interaction between CuPc and RGO due to the reduction of epoxy groups in graphene sheets (Fig. 2).

After treating under solvothermal condition, the further red-shift in S-RGO/CuPc can be observed while the Q-band of S-GO/CuPc also displays a conspicuous red-shifts in comparison with that of CuPc (Fig. 4b, c), reflecting the further enhanced π – π interaction between graphene and CuPc [24], which also confirms that GO and/or RGO is successfully reduced under solvothermal condition. The labile oxygen functional groups (hydroxyl and/or uncoordinated epoxy groups) within GO or RGO are broken away during solvothermal process as discussed in Fig. 2, leading to restoration of π -electron within the graphene, thereby enhancing the π – π interaction between graphene and CuPc. Interestingly, the red-shift of Q-band of S-RGO/CuPc is more distinct than that of S-GO/CuPc (Table 2),

suggesting stronger π – π interaction in S-RGO/CuPc. It can be attributed to prior reduction of epoxy groups by using hydrazine monohydrate besides solvothermal reduction. Based on the results of XPS (Fig. 2), the reduction degree of epoxy groups under solvothermal conditions is similar to that reduced by hydrazine monohydrate. Thus, the difference confirms the existence of metal–ligand coordination between GO and CuPc, which will hinder the breakaway of epoxy groups in GO/CuPc under solvothermal condition. For H₂Pc, Q-band splits into two peaks at 671 nm (Q₁) and 702 nm (Q₂) (Fig. 3d; Table 3) [25]. When incorporated with GO, the similar red-shift evolution occurs in the Q₁-band of H₂Pc, which can be also due to the enhancing π – π interaction between graphene sheets and H₂Pc molecules.

3.4 Morphology of the graphene/phthalocyanine nanocomposites

The SEM micrographs of graphene/phthalocyanine composites were also characterized and shown in Fig. 5. For comparison, GO is consisted of thin, flat, and randomly crumpled sheets as depicted in Fig. 6 [26]. For U-GO/CuPc, sphere-like embossments with a diameter of ~40 nm homogeneously and tightly disperse on the surface of graphene sheets (Fig. 5a). The formation of this hetero-structure indicates that GO/CuPc nanocomposites are successfully fabricated by self-assembling of CuPc on the graphene sheets. As to U-RGO/CuPc, similar surface morphology can be observed (Fig. 5c). However, the micrograph of U-RGO/CuPc shows lower density of embossments with a bigger size of ~50 nm on the surface of graphene sheets, which once again verifies the difference in interaction between U-GO/CuPc and U-RGO/CuPc. Interestingly, the surface of U-GO/H₂Pc appears relatively flat, with H₂Pc densely and evenly lay on the surface of graphene sheets, and none of the sphere-like nanostructure is observed (Fig. 5e). The difference in morphology can be identified as a result of the competition between metal–ligand coordination and π – π interaction between GO and CuPc, indirectly confirming the existence of metal–ligand coordination between GO and CuPc. After the solvothermal treatment, the embossments lay on the surface of the graphene sheets evolve into sphere-like nanoparticles with clear profile while the S-GO/CuPc still displays a higher dispersion density of nanoparticles than S-RGO/CuPc as revealed in Fig. 5b, d. As to S-GO/H₂Pc, no obvious change appears in micrograph (Fig. 5f).

GO, as an important precursor of graphene, possesses a large 2D planar structure, which consists of two parts: oxygen-functional groups and graphitic domain as presumed in Fig. 7 [27]. Upon self-assembling, the local delocalized π -electron system of graphitic domain effectively

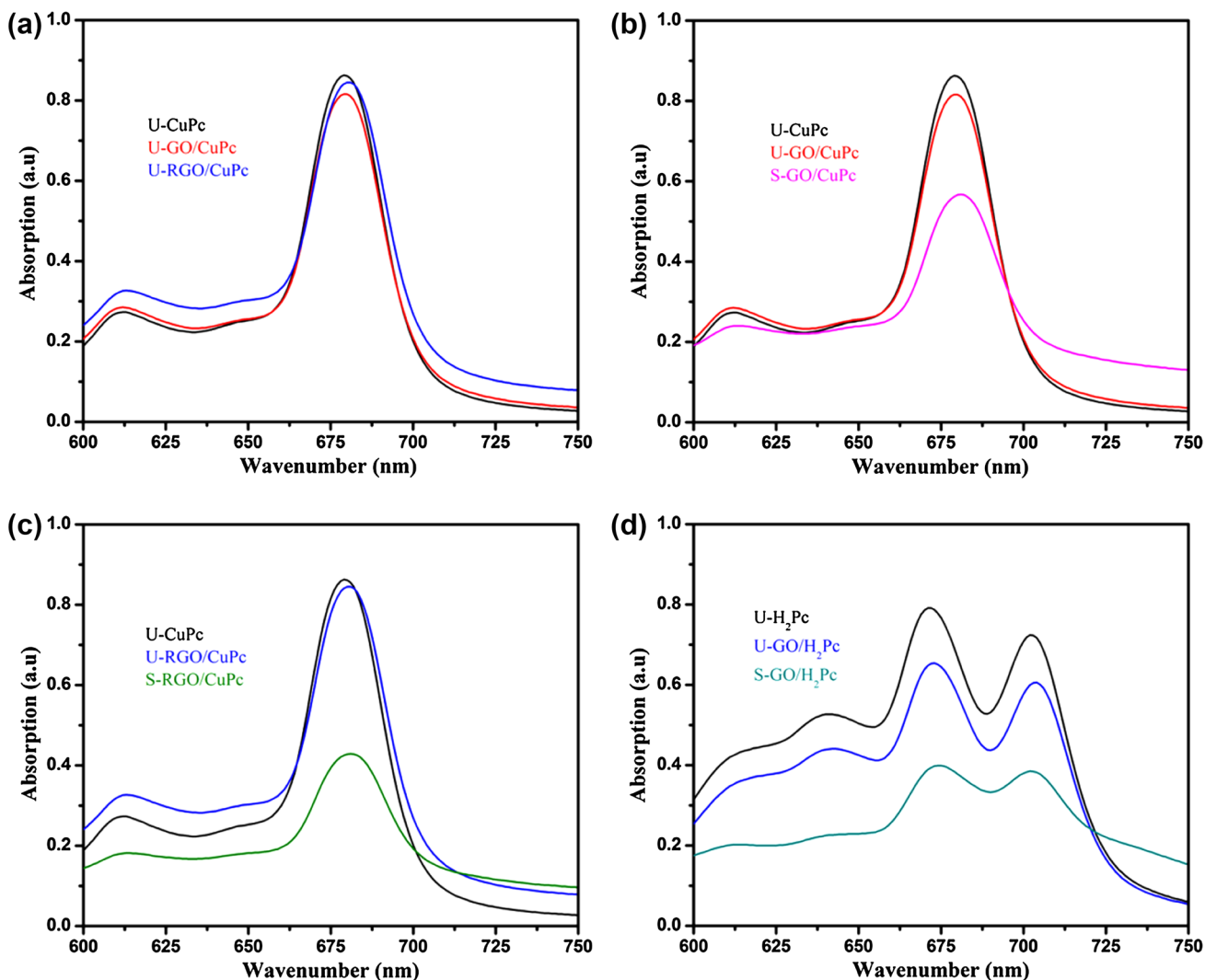


Fig. 4 UV–Vis spectra (a) of U-CuPc, U-GO/CuPc and U-RGO/CuPc and the corresponding results (S-GO/CuPc (b), S-RGO/CuPc (c) and S-GO/H₂Pc (d)) of samples in NMP

Table 2 The Q-band in UV–Vis curves of U-CuPc, U-GO/CuPc and U-RGO/CuPc dispersions in NMP

	Q-band (nm)
U-CuPc	679.0
U-GO/CuPc	679.4
S-GO/CuPc	680.8
U-RGO/CuPc	680.6
S-RGO/CuPc	681.4

Table 3 The Q-band in UV–Vis curves of GO/H₂Pc dispersions in NMP

	Q ₁ -band (nm)	Q ₂ -band (nm)
U-H ₂ Pc	671.0	702.0
U-GO/H ₂ Pc	673.2	703.8
S-GO/H ₂ Pc	674.0	702.4

facilitates interaction with CuPc (H₂Pc) through the π – π stacking interaction, which can be confirmed by the results of UV–Vis spectra (Fig. 4). As a result, CuPc (H₂Pc) molecules tightly lay on the surface of graphene sheets as shown in Fig. 5. On the other hand, the oxygen-functional groups of GO and/or RGO, especially the carboxyl and epoxy species, tend to act as a ligand that coordinated with the central metal ions of CuPc [14, 15], which can be confirmed by the results of XPS spectra (Fig. 3). As a kind of special covalent bond, the formation of metal–ligand coordination bond realizes the effective linkage between graphene sheet and CuPc molecule, acting as a reactive site that drives the CuPc aggregates to form the sphere-like embossments on GO sheets as shown in Fig. 5a, c. Meanwhile, the solvothermal environment further facilitates the CuPc embossments “growing” into sphere-like nanoparticles with a

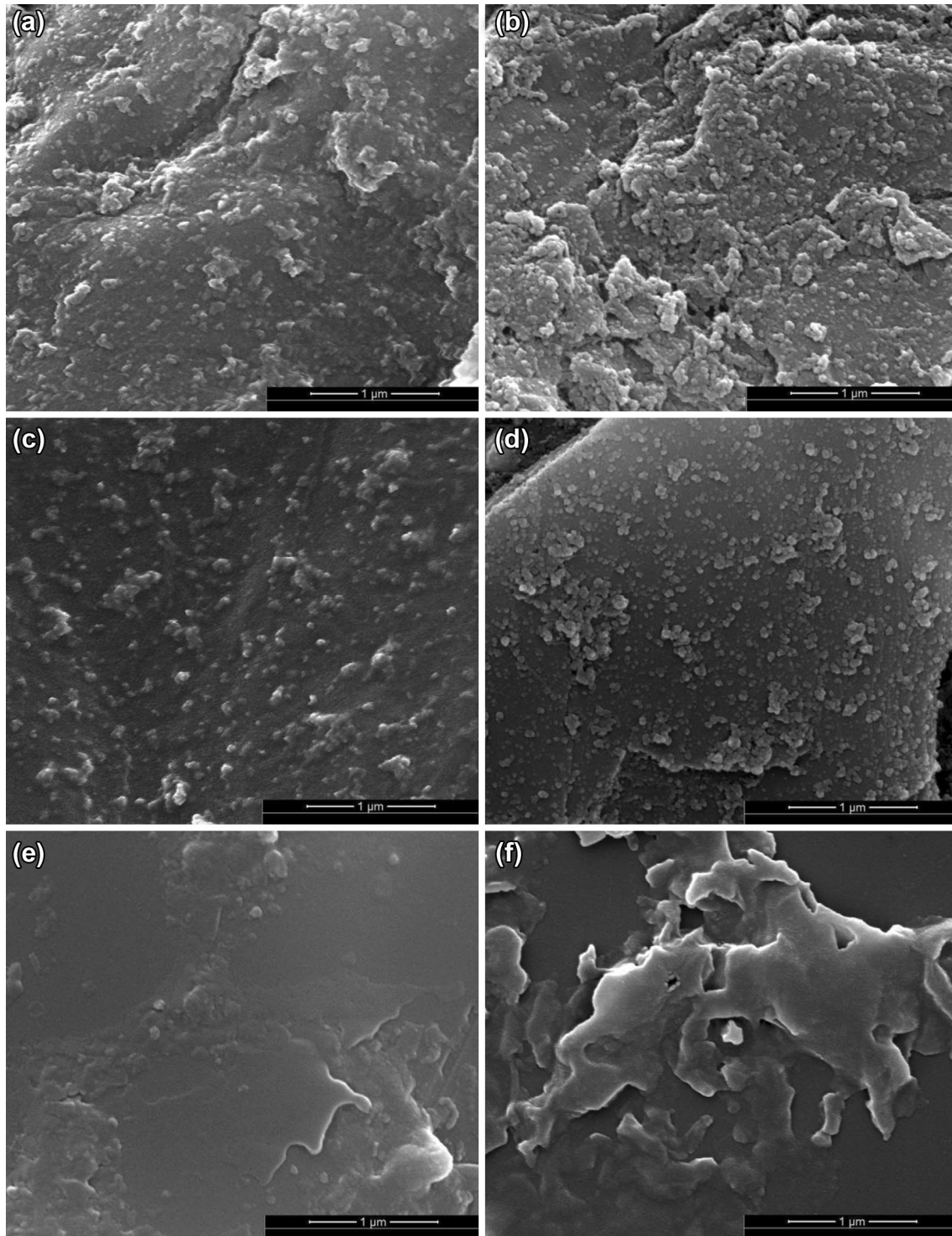


Fig. 5 SEM images of U-GO/CuPc (a), U-RGO/CuPc (c) and U-GO/H₂Pc (e); and the corresponding images of S-GO/CuPc (b), S-RGO/CuPc (d) and S-GO/H₂Pc (f)

bigger size as emerged in Fig. 5b, d. For RGO/CuPc system, the weakened metal–ligand coordination due to the prior reduction of epoxy groups finally results in the

decrement in dispersing density of nanospheres. As to GO/H₂Pc only controlled by π – π interaction as the absence of Cu in H₂Pc, none of the sphere-like nanostructure appears

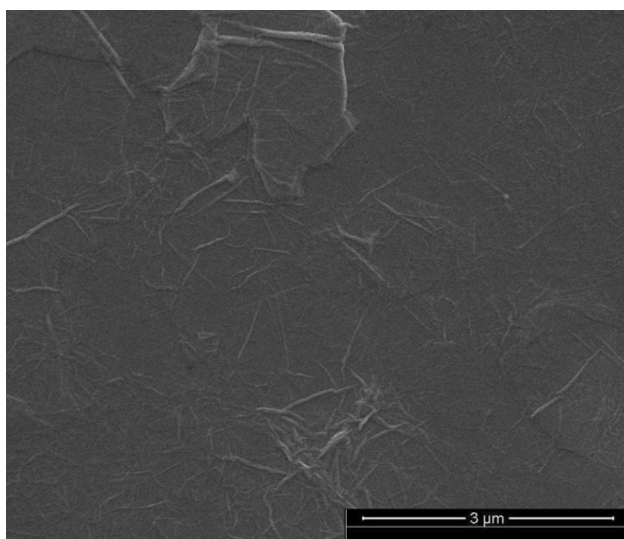


Fig. 6 SEM images of GO sheets

on graphene sheets as shown in Fig. 5e, f. Thus, it can be concluded that the the formation of metal–ligand coordination synergized with π – π interaction effectively facilitates the fabrication of GO/CuPc nanocomposites by self-assembling of CuPc on the graphene sheets, whereas the competition between metal–ligand coordination and π – π interaction between graphene and phthalocyanine endow composites with conspicuous evolutions in self-assembly behaviors and morphology.

3.5 Dielectric properties and alternating current (AC) conductivity of the graphene/phthalocyanine nanocompoistes

The dielectric properties of the obtained nanocomposites were also studied by measuring dielectric constant, dielectric loss and alternating current (AC) conductivity at room temperature using an electric double layer method. From Fig. 8a, U-GO/CuPc and U-GO/H₂Pc exhibit almost the same dielectric constant (~4) as those of CuPc and H₂Pc. For U-RGO/CuPc, the dielectric constant is improved to 6.54 at 1 kHz with an increment of 64% in comparison with that of pure CuPc (3.98 at 1 kHz), which can be attributed to the reduction of epoxy groups in RGO [12]. High aspect ratios and large surface area of flake-like graphene oxide make it possible to form a nanocapacitor structure with the adjacent CuPc.

Interfacial polarization, known as Maxwell–Wagner–Sillars (MWS) polarization, arises from electrical heterogeneous materials between GO and CuPc in which the conductivity of CuPc matrices and GO are different. In these materials, the motion of the charge carriers may occur more easily through one phase and therefore are constricted at phase boundaries. The accumulation of free charges and the formation of dipoles at the interfaces result in the increase of the dielectric constant. For the insulating GO, the improvement in dielectric constant by introducing GO into CuPc matrices is slight as shown in Fig. 8a. But for RGO reduced by hydrazine monohydrate, the restoration of π -electron within the graphene

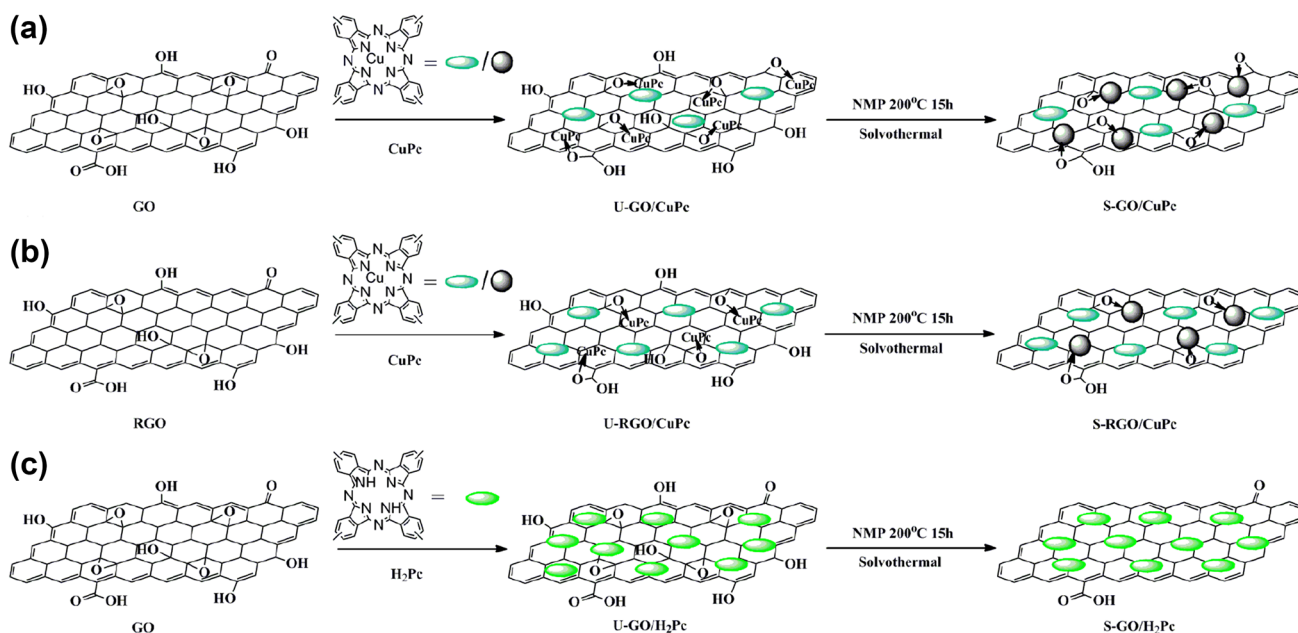


Fig. 7 Schematic representation of fabricating nanocomposites with different morphologies and performances: **a** GO/CuPc; **b** RGO/CuPc and **c** GO/H₂Pc

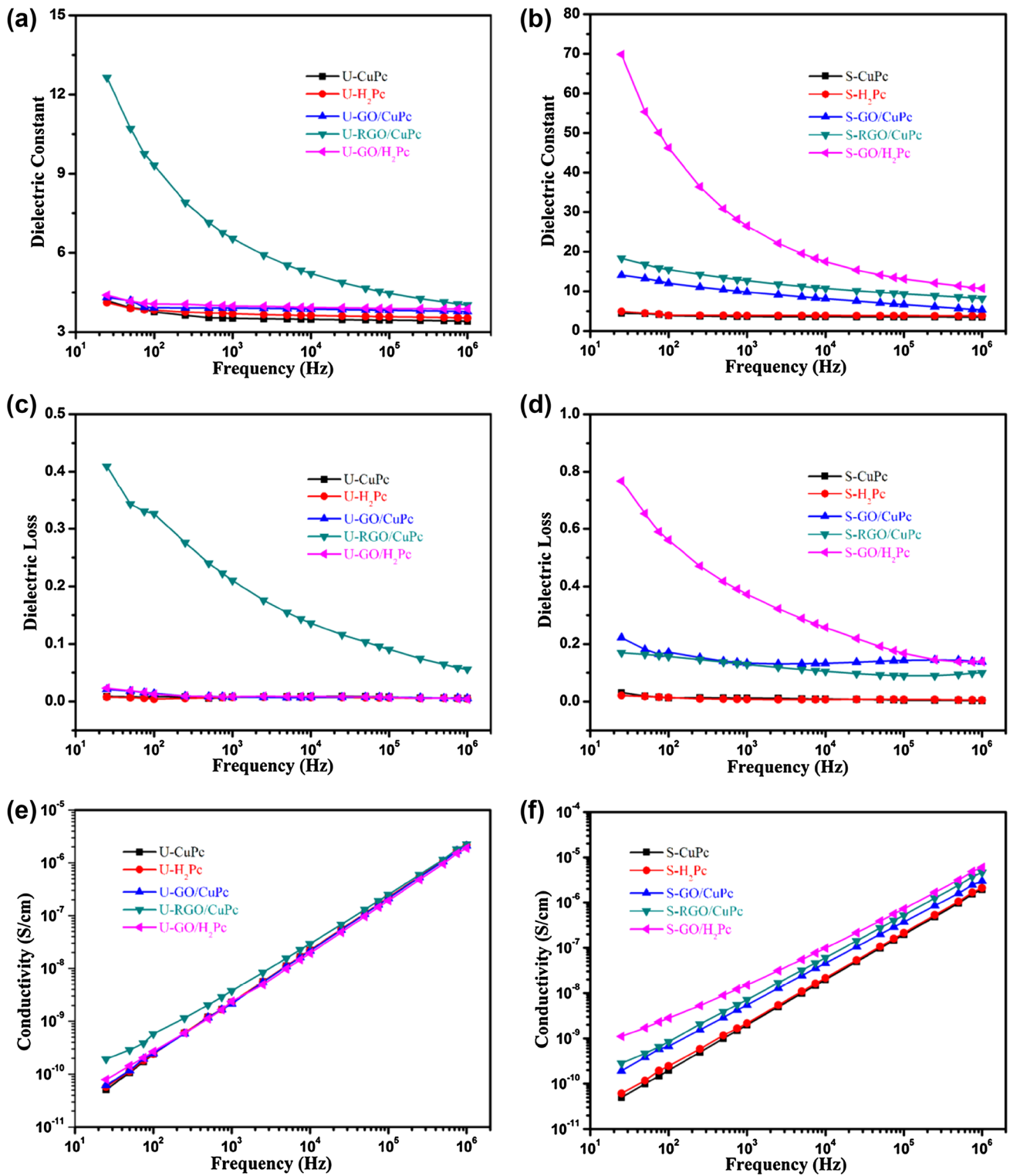


Fig. 8 Dielectric constant (a), dielectric loss (c) and AC conductivity (e) of U-CuPc, U-H₂Pc, U-GO/CuPc, U-RGO/CuPc and U-GO/H₂Pc; (b), (d) and (f): the corresponding parameters of S-CuPc, S-H₂Pc, S-GO/CuPc, S-RGO/CuPc and S-GO/H₂Pc settled on the right

contributes to improvement in electrical conductivity of GO sheets. The increased mismatch in conductivity between the two phases of RGO and CuPc results

in that more and more free charge carriers accumulate at the interface and give rise to a strong MWS interfacial polarization, leading to the obvious increase in the

dielectric constant [28]. Meanwhile, the similar trends of AC conductivity can be observed in Fig. 8e. After the solvothermal treatment, the dielectric constant exhibits drastic evolution as shown in Fig. 8b. Especially, the dielectric constant and AC conductivity of S-GO/H₂Pc is as high as 26.53 and 1.51×10^{-8} S/cm at 1 kHz, with a sharp increment of 565 and 534% comparing with that of U-GO/H₂Pc, which is higher than that of S-RGO/CuPc (12.68 and 3.77×10^{-9} S/cm at 1 kHz) and S-GO/CuPc (9.83 and 2.15×10^{-9} S/cm at 1 kHz). The difference in dielectric constant and AC conductivity can be also identified as a result of the competition between metal–ligand coordination and π – π interaction between GO and CuPc. The substantially improvement of GO/H₂Pc can be attributed to the absence of metal–ligand coordination bond between GO sheet and metal-free phthalocyanine, resulting in unhindered breakaway of the labile oxygen-functional groups (hydroxyl and/or uncoordinated epoxy groups) of GO during the solvothermal process (as discussed in Fig. 2), thereby maximum restoring the electrical conductivity of graphene. As a result, the formation of the strongest MWS interfacial polarization finally causes the most drastic improvement in the dielectric constant and AC conductivity of the system. For others, the formation of metal–ligand coordination bond hinders the conductivity restoration of GO sheets during the solvothermal process, weakening the MWS interfacial polarization, leading to the improvement in dielectric constant and AC conductivity becoming pallid as shown in Fig. 8b, f. Meanwhile, it is worth noting that S-RGO/CuPc displays a distinct superiority in dielectric constant to S-GO/CuPc, which can be also identified to the result of the competition between metal–ligand coordination and π – π interaction between GO and CuPc. The weakened metal–ligand coordination and enhanced π – π interaction between RGO and CuPc in U-RGO/CuPc further facilitate the accumulation of more free charges at the interface, thereby obtaining a higher dielectric constant and AC conductivity for S-RGO/CuPc than that of S-GO/CuPc, due to the prior reduction of epoxy groups in RGO by using hydrazine monohydrate. In addition, under the alternating electrical field, interfacial relaxation would be established due to the delay of the induced charges which counters the external applied field and the electrical energy is dissipated subsequently as heat energy, so the dielectric loss occurs and exhibits the similar trends as that of dielectric constant and AC conductivity as shown in Fig. 8c, d. Based on the above, it can conclude that the restoration of the π -electron within the graphene will effectively enhance the dielectric properties and AC conductivity of the GO/CuPc and its derivatives nanocomposites, whereas the formation of metal–ligand

coordination bond will impede the improvement in dielectric properties.

4 Conclusions

In summary, graphene/phthalocyanine derivatives were successfully prepared by self-assembling of phthalocyanine on graphene oxide under solvothermal condition. The obtained composites presented different evolutions in self-assembly behavior, morphologies and dielectric properties due to the changing in the relative intensity of π – π stacking interaction and metal–ligand coordination in them. Importantly, the formation of metal–ligand coordination bond between GO and CuPc hindered the improvement of dielectric properties of the composites while the effective restoration of the π -electron within the graphene played a dominant role in enhancing the dielectric properties and AC conductivity, which provided a facile guidance to prepare graphene/phthalocyanine composites with high dielectric properties.

Acknowledgements The financial supports from National Natural Science Foundation of China (Project NoS. 51373028, 51403029), South Wisdom Valley Innovative Research Team Program and Ningbo Major (key) Science and Technology Research Plan (2013B06011) are gratefully acknowledged.

References

1. M. Ouyang, R. Bai, L. Chen, L.G. Yang, M. Wang, H.Z. Chen, J. Phys. Chem. C **112**, 11250–11256 (2008)
2. R. Zhao, H.L. Tang, H. Guo, Y.J. Lei, X.B. Liu, J. Mater. Res. **28**, 1609–1616 (2013)
3. S.C. Suen, W.T. Whang, F.J. Houand, B.T. Dai, Org. Electron. **7**, 428–434 (2006)
4. M.Y. Zhang, C.L. Shao, Z.C. Guo, Z.Y. Zhang, J.B. Mu, T.P. Cao, Y.C. Liu, ACS Appl. Mater. Interf. **3**, 369–377 (2011)
5. S. Choi, S.H. Hong, S.H. Cho, S. Park, S.M. Park, O. Kim, M. Ree, Adv. Mater. **20**, 1766–1771 (2008)
6. S. Rajaputra, S. Vallurupalli, V.P. Singh, J. Mater. Sci. **18**, 1147–1150 (2007)
7. M. Guo, X.Z. Yan, III.T. Goodson, Adv. Mater. **20**, 4167–4171 (2008)
8. M.S. Go, J.M. Song, C. Kim, J. Lee, J. Kim, M.J. Lee, Electron. Mater. Lett. **11**, 252–258 (2015)
9. X. Zhao, R. Zhao, X.L. Yang, J.C. Zhong, X.B. Liu, J. Elect. Mater. **40**, 2166–2171 (2011)
10. M. Guo, X.Z. Yan, Y. Kwon, T. Hayakawa, M. Kakimoto, III.T. Goodson, J. Am. Chem. Soc. **128**, 14820–14821 (2006)
11. M. Guo, T. Hayakawa, M. Kakimoto, III.T. Goodson, J. Phys. Chem. B **115**, 13419–13432 (2011)
12. H.X. Tang, G.J. Ehlert, Y.R. Lin, H.A. Sodano, Nano Lett. **12**, 84–90 (2012)
13. Y.H. Li, M. Fan, K. Wu, F.L. Yu, S.G. Chai, F. Chen, Q. Fu, Compos. Part A **73**, 85–92 (2015)

14. J.H. Yang, Y.J. Gao, W. Zhang, P. Tang, J. Tan, A.H. Lu, D. Ma, *J. Phys. Chem. C* **117**, 3785–3788 (2013)
15. F.B. Meng, X.B. Liu, *RSC Adv.* **4**, 8699–8702 (2014)
16. D.C. Marcano, D.V. Kosynkin, J.M. Berlin, A. Sinitskii, Z.Z. Sun, A. Slesarev, L.B. Alemany, W. Lu, J.M. Tour, *ACS Nano* **4**, 4806–4814 (2010)
17. S. Park, J. An, I. Jung, R.D. Piner, S.J. An, X.S. Li, A. Velamakanni, R.S. Ruoff, *Nano Lett.* **9**, 1593–1597 (2009)
18. L. Xu, G. Xiao, C. Chen, R. Li, Y. Mai, G. Sun, D. Yan, *J. Mater. Chem. A* **3**, 7498–7504 (2015)
19. S.J. Park, K.S. Lee, G. Bozoklu, W.W. Cai, S.T. Nguyen, R.S. Ruoff, *ACS Nano* **2**, 572–578 (2008)
20. S.C. Kim, G.B. Lee, M.W. Choi, Y. Roh, C.N. Whang, K. Jeong, J. Lee, S. Kim, *Appl. Phys. Lett.* **78**, 1445–1447 (2001)
21. J. Marsh, L. Minel, M.G. Barthes-Labrousse, D. Gorse, *Appl. Surf. Sci.* **133**, 270–286 (1998)
22. A. Chunder, T. Pal, S.I. Khondaker, L. Zhai, *J. Phys. Chem. C* **114**, 15129–15135 (2010)
23. K. Jia, R. Zhao, J.C. Zhong, X.B. Liu, *J. Mater. Sci.* **21**, 708–712 (2010)
24. D. Sergey, G. Scott, W. Kan, C.T. Vincent, C. Kitty, S.H. Anthony, F. Jabari, V. Rupal, Y. Yang, B.K. Richard, *ACS Nano* **4**, 3845–3852 (2010)
25. H.Y. Yenilmez, İ. Özçesmeçi, A.İ. Okur, A. Gül, *Polyhedron* **23**, 787–791 (2004)
26. T.T. Xiao, C.L. Yang, Y.G. Lu, F.L. Zeng, *J. Mater. Sci.* **25**, 3364–3374 (2014)
27. Y.C. Si, E.T. Samulski, *Nano Lett.* **8**, 1679–1682 (2008)
28. B.D. Chin, Y.S. Lee, O.O. Park, *J. Coll. Interface Sci.* **201**, 172–179 (1998)